

# Two-dimensional MHD models of solar magnetogranulation. Testing of the models and methods of Stokes diagnostics

V.A. Sheminova

Main Astronomical Observatory, National Academy of Sciences of Ukraine  
Zabolotnoho 27, 03689 Kyiv, Ukraine

## Abstract

We carried out the Stokes diagnostics of new two-dimensional magnetohydrodynamic models with a continuous evolution of magnetogranulation in the course of two hours of the hydrodynamic (solar) time. Our results agree satisfactorily with the results of Stokes diagnostics of the solar small-scale flux tubes observed in quiet network elements and active plages. The straightforward methods often used in the Stokes diagnostics of solar small-scale magnetic elements were tested by means of the magnetohydrodynamic models. We conclude that the most reliable methods are the determination of magnetic field strength from the separation of the peaks in the Stokes V profiles of the infrared Fe I line 1564.8 nm and the determination of the magnetic inclination angle from the ratio  $\tan^2 \gamma \approx (Q^2 + U^2)^{1/2} / V^2$ . The lower limits for such determinations are about 20 mT and  $10^\circ$ , respectively. We also conclude that the 2D MHD models of solar magnetogranulation are in accord with observations and may be successfully used to study magnetoconvection in the solar photosphere.

## 1 Introduction

Solar small-scale flux tubes still remain spatially unresolved. In this case the Stokes diagnostics is the only available technique for the investigation of their structure and dynamics. The straightforward methods of Stokes diagnostics [17, 20, 21] allow the necessary information to be obtained after simple calculations from direct measurements of the observable Stokes profile parameters. The inversion methods [2, 14] are used to construct flux tube models by fitting synthetic Stokes profiles to the observed ones. The methods of numerical calculation of magnetoconvection in the photospheric layers [1, 5, 7] and construction of self-consistent nonstationary magnetohydrodynamic models have also been developed. The MHD models are very useful in studying physical processes in solar magnetic features, but they cannot be directly compared to observations.

We attempted to make such comparison, using the Stokes diagnostics. In this paper we match new two-dimensional MHD models [6] to observations and examine the reliability of the Stokes diagnostics based on the MHD models.

## 2 Calculations

The MHD models used in our study are described in detail in [6]. The model sequence starts with a convective model with an initial average magnetic field of about 5 mT and terminates at the moment 120 min with an average field of 50 mT. The sequence contains 94 2-D models with a 1-min interval and 52 models with a 0.5-min interval between them. The simulation region is a rectangle of length  $x = 3920$  km and height  $h = 1820$  km, it contains 112 vertical columns (rays) spaced at 35-km intervals. All the atmospheric thermodynamic parameters necessary for calculating the equations of radiative transfer in spectral lines for every such column in the presence of magnetic fields were put at our disposal by A. S. Gadun.

The transfer equations for polarized radiation in each of 112 columns were solved in the LTE approximation for a plane-parallel atmosphere, and the Stokes profiles obtained in the solution were averaged over space. The equations were solved numerically by a modified method [11] which is described in detail by Sheminova [16]. The Stokes profiles were calculated for three Fe I lines in the visible ( $\lambda\lambda$  524.71, 525.02, 525.06) and one line in IR ranges ( $\lambda$  1564.85 nm).

## 3 Comparison of MHD models with observations

The validity of any numerical simulation can be confirmed only by observation data. The MHD models used here may be quite adequate in their parameters to solar small-scale magnetic elements. We can calculate the Stokes profile parameters for these models and compare them to the data of spectropolarimetric observations. For this purpose we use the Stokes profiles observed in quiet network elements and active plages with a Fourier spectrograph at the McMath telescope in 1979 [24]. The chief value of these data is that a large number of spectral lines were observed simultaneously in the wavelength range 445–557 nm with a high spectral resolution (420000). Unfortunately, the spatial and temporal resolutions were not high (10" and 35–52 min). Out of 402 iron lines, we selected 170 unblended lines with known laboratory wavelengths. We calculated absolute shifts for the I and V profiles of these lines, using the strong Mg I 517.2 nm line as a reference line and the laboratory wavelength system by Pierce and Breckinridge [13]. The magnetic field strength was calculated for every line by the method of the center of masses [15]. We also determined the asymmetry of amplitudes and areas in the observed V profiles. Thus we acquired the necessary observational data which could be used to check the results of theoretical simulations of magnetoconvection in the photospheric layers.

The time series of MHD models selected for comparison with observations extended over the simulation period from 95 min to 120 min. We calculated the Stokes profiles of four spectral lines for each column in the simulation region in each of 52 models (at 0.5-min intervals); we obtained about 5800 profiles for every line. This procedure is analogous to an observation of the Stokes profiles by scanning a very narrow region 3920 km long on the solar surface with a spatial resolution of 35 km at 0.5-min intervals in the course of 25 min with instantaneous exposures. For each calculated profile we determined the same parameters as for the observed profiles. A preliminary analysis revealed that the profiles of the weak IR line 1564.8 nm were the best suited for the comparison. This line forms deep in the photosphere ( $\log \tau_R$  from 0 to -1), it is the least sensitive to temperature fluctuations [20] and is virtually unaffected by saturation. The other three lines, in the visible range, are formed high in the photosphere ( $\log \tau_R$  from -2 to -4), their central in-

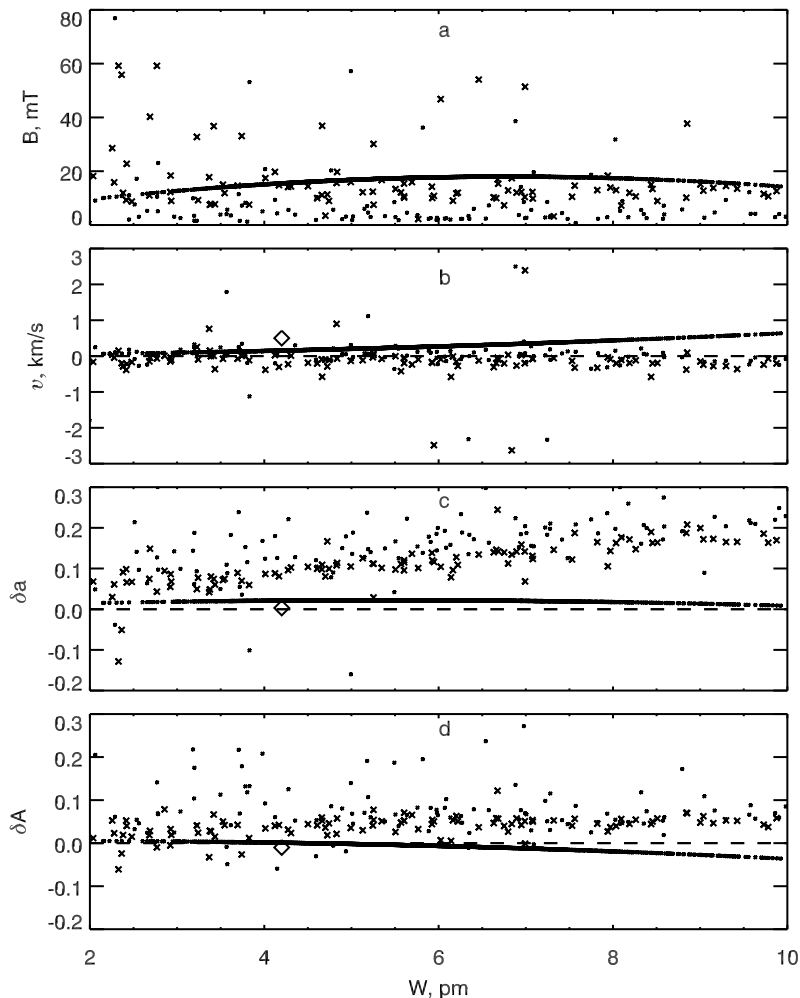


Fig. 1. Comparison of the results of Stokes diagnostics of MHD models (solid line) and observations in the quiet network features (squares) and active plages (crosses): a) field intensity, b) absolute shift, c) asymmetry of V-profile amplitudes, d) asymmetry of V-profile areas.

tensities are temperature-sensitive, they are also sensitive to saturation and NLTE effects. The data for the uppermost layers, which depend on boundary conditions to a greater extent, are less reliable in our MHD models. The visible lines formed in the upper layers are supersaturated, as a rule, and their diagnostic capabilities are drastically impaired.

Figure 1 displays the magnetic field strength  $B$ , absolute shift  $v$ , asymmetry of amplitudes and areas,  $\delta a$  and  $\delta A$ , as functions of equivalent width; the quantities obtained from the observed V profiles are shown by squares and crosses, and the calculated parameters are represented by the second-order curves (average values from 5800 IR line profiles). We did not expect a complete agreement between the observed and calculated parameters, since there were some distinctions in resolution, line sampling, and selection of observation regions. The observed Stokes profiles were measured in magnetic features only, while the calculated profiles referred to the entire simulation region. Only 30 percent of calculated scans, in the best case, may be referred to magnetic elements. It is seen from Fig. 1 that the calculated values of  $B$  and  $v$  fall within the observed intervals, while the asymmetries of amplitudes and areas are smaller, on the average, than in the observed profiles. This might be attributed to the well-known observation facts [12]. In the quiet network elements the measured asymmetries  $\delta a$  and  $\delta A$  for 1564.8 nm are close to zero (big diamonds in Fig. 1). An interpretation for these facts can be found in [7]. Despite some differences, we may conclude that realistic Stokes profile parameters are derived within the framework of the MHD models, they are close to the parameters observed in the quiet network elements and plages.

## 4 Reliability of Stokes diagnostics

To test the methods of Stokes diagnostics, we selected one 2-D model (snapshot) from the MHD model sequence [6], namely, the model corresponding to the 120th min of simulation time.

Figure 2 demonstrates the distribution of various parameters in the simulation region: isotherms, isobars, velocity field, and field strength, together with the field lines and polarity. Two flux tubes of various strengths and polarities with clearly defined strong longitudinal fields stand out in the simulation region; an area at the granule center, where a new flux tube begins to form, can be also clearly seen. With these data, we calculated the Stokes profiles of four spectral lines for each of 112 model columns (scans) and applied various methods of Stokes diagnostics with the aim to determine the flux tube parameters. We examine the agreement between the quantities thus obtained and the thermodynamic model parameters and the observation data for magnetic elements.

### 4.1 Magnetic field strength

There are three methods for the determination of this parameter. The first method is based on the ratio of the amplitudes  $a_V$  of the V profiles of two lines in the visible range with various Zeeman splittings and similar other parameters [22, 23]:

$$\text{MLR} = \frac{a_V(525.02)g_{\text{eff}}(524.71)}{a_V(524.71)g_{\text{eff}}(525.02)} \approx \frac{2}{3} \cdot \frac{a_V(525.02)}{a_V(524.71)}.$$

Traditionally, the observed magnetic line ratio (MLR) is calibrated with the use of simple models with homogeneous magnetic fields;  $\text{MLR} = 1$  for weak fields, and  $\text{MLR} < 1$  for strong fields. This ratio may be greater than unity in the regions where the saturation in the cores of strong lines weakens the V profile. When the velocity, which broadens the profiles, increases, the MLR may also increase. This degrades the reliability of the field strength determined for flux tubes and makes more stringent the requirements imposed on the MLR calibration.

In the method of the centers of mass the longitudinal field strength is estimated from the measurements of the central wavelengths of positively and negatively polarized line components [15].

$$\lambda_{\pm} = \frac{\int [I_c - (I_c \pm V)] \lambda d\lambda}{\int [I_c - (I_c \pm V)] d\lambda}$$

The field strength  $B$  (in tesla) is readily found from the well-known expression for the Zeeman splitting:

$$B_{rb} = (\lambda_- - \lambda_+) / (2 \cdot 4.67 \cdot 10^{-8} \lambda_0^2 g_{\text{eff}}), \quad (1)$$

$\lambda_0$  being the line wavelength (in nanometers). This method is quite reliable for the solar disk center, but it gives only the lower limit of  $B$ , as it specifies the longitudinal field component only.

The third method is the simplest one — it is based on the measurement of the distance  $\Delta\lambda_{br}$  between the peaks in the red (r) and blue (b) wings of the V profile of the IR line with the Landé factor equal to 3. This is a very efficient method [9, 20]. With expression (1), we can derive the field strength  $B_{br}$  as the upper limit. As the quantity  $\Delta\lambda_{br}$  consists

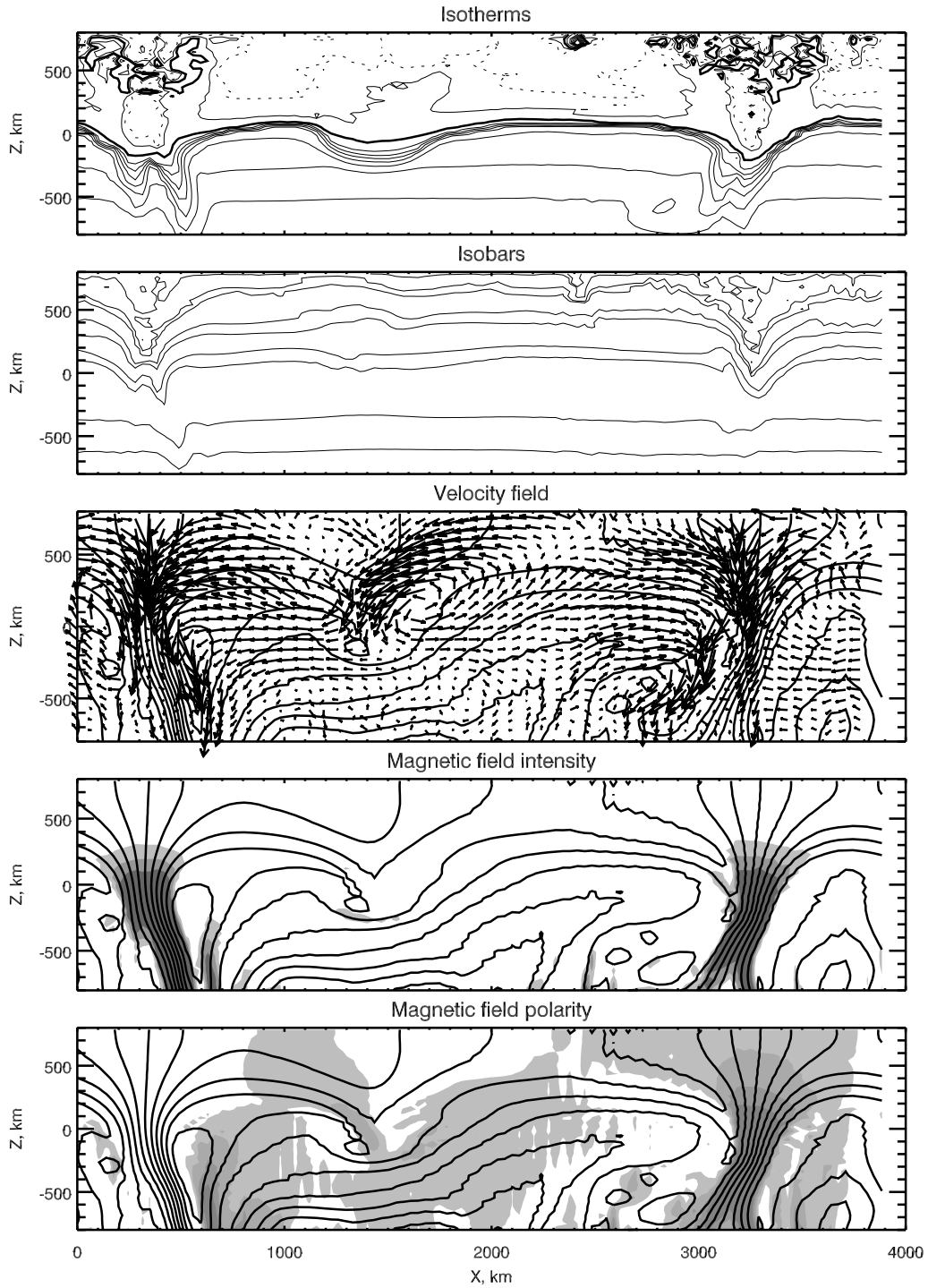


Fig. 2. Snapshots from 2D MHD models [6] at simulation moment 120 min. Isotherms for every 1000 K: dotted line) 4000 K and thick line) 6000 K. The latter roughly indicates the level  $\log \tau_R = 0$ . Magnetic field lines are shown in three lower panels. Magnetic field intensity: hatching density is proportional to intensities of 0, 80, 110, and 140 mT. Magnetic field polarity: hatching density corresponds to field intensities of 1, 40, 80, and 120 mT in the positive polarity field.

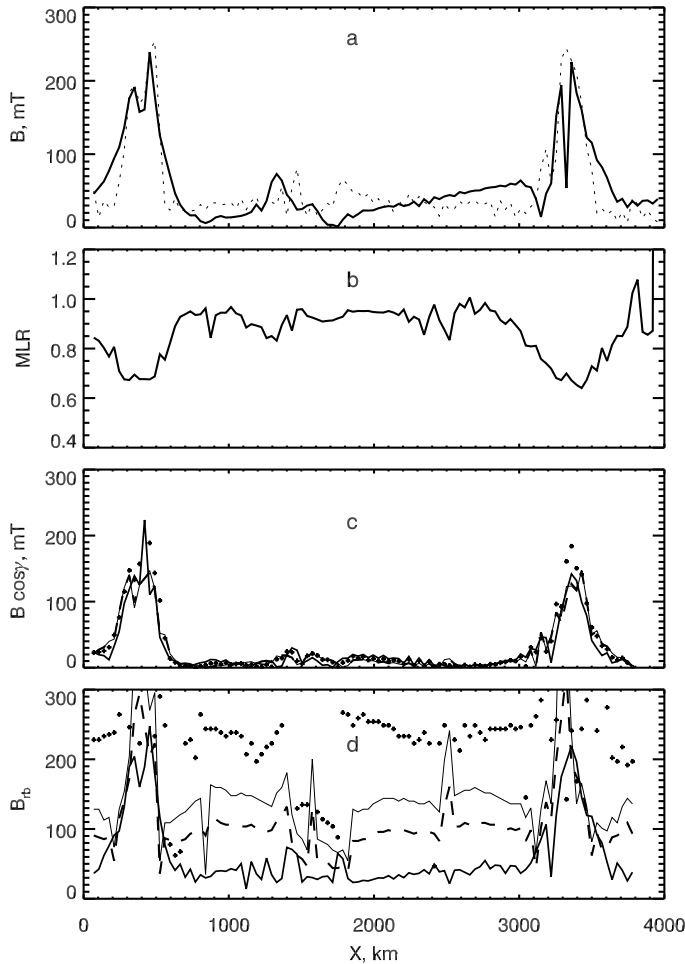


Fig. 3. Magnetic field intensity  $B$  along the simulation region: a) from a MHD snapshot at the levels  $\log \tau_R = 0$  (solid line) and  $\log \tau_R = -2$  (dotted line); b) line ratio method; c) method of center of masses; d) method based on the distance between the V-profile peaks. For c) and d) thick line shows the data derived from  $\lambda 1564.85$  nm, thin line from  $\lambda 524.71$  nm, dashed line from  $\lambda 525.02$  nm, and plusses from  $\lambda 525.06$  nm.

of the Doppler line width  $\Delta\lambda_D$  and the Zeeman splitting  $\Delta\lambda_H$ , the distance between the V-profile peaks in weak fields, when the first component is prevailing, is determined mainly by the nonmagnetic line width, i.e, it is practically independent of magnetic field. As the field increases, the Zeeman splitting becomes prevailing. That is the reason why this method fails in the case of very weak photospheric fields.

One can see in Fig. 3a the variations in the model field strength at the photosphere levels  $\log \tau_R = 0$  and  $\log \tau_R = -2$ . The maximum field strength in the model flux tubes at  $\log \tau_R = 0$  is as large as 200–250 mT in a very narrow interval (35–70 km). It is known from observations (their resolution is no better than 200 km) that the field strength at  $\log \tau_R = 0$  is 100–150 mT in magnetic elements and 150–200 mT in pores, less than in the model flux tubes.

Figures 3b-d show the field strength determined by three methods. The best fit to the model values of  $B$  is provided by the third method (distance between the V-profile peaks) with the use of the IR line Fe I 1564.8 nm (Fig. 3d). The lower limit for the measurements by this method is about 20 mT. The line ratio method (Fig. 3b) becomes less reliable at about 0.1 T, MLR being equal to 0.65–0.7 in this case. The method of the center of masses (Fig. 3c) allows longitudinal magnetic fields to be measured, and their strength obviously depends on the inclination of field lines in flux tubes. A greater inclination in the second tube as compared to the first tube results in an underestimate of about 70 mT at the level  $\log \tau_R = 0$ .

## 4.2 Magnetic field inclination

The angle  $\gamma$  of the field vector and the line of sight can be found directly from the relations for the amplitudes of  $\sigma$ -components in the V, Q, and U profiles [3, 17]:

$$V \approx \cos \gamma, \quad Q \approx \sin^2 \gamma \cos^2 \chi, \quad U \approx \sin^2 \gamma \sin^2 \chi,$$

$$\frac{\sqrt{Q^2 + U^2}}{V} \approx \frac{\sin^2 \gamma}{\cos \gamma}, \quad \frac{U}{Q} = \tan^2 \chi.$$

Here  $\chi$  is the field vector azimuth. These relations are valid when the observed line is weak and the angles  $\gamma$ ,  $\chi$  do not change along the line of sight. The ratio  $(Q^2 + U^2)^{1/2}/V$  depends on wavelength, field strength, line saturation, etc. [20].

In strong magnetic fields the amplitudes of V, Q, and U profiles do not depend on  $B$  due to magnetic saturation of lines, and therefore  $\gamma$  can be reliably determined. In weak fields,  $V \approx B$  and Q and U are of the order of  $B^2$ , and the ratio depends not only on  $\gamma$  but on  $B$  as well. In actual practice this ratio is calibrated with the use of model calculations. In our two-dimensional MHD models the magnetic vector azimuth is equal to zero or  $180^\circ$  and  $U \approx 0$ . Although the U profile does not vanish altogether due to magneto-optical effects, it is very small, and it may be ignored. The angle  $\gamma$  can be derived directly from the amplitude ratio when the ratio  $(Q^2 + U^2)^{1/2}/V$  is divided by V and  $U = 0$  is substituted:

$$\frac{\sqrt{Q^2 + U^2}}{V^2} \approx \frac{\sin^2 \gamma}{V \cos \gamma} = \tan^2 \gamma, \quad \frac{Q}{V^2} \approx \tan^2 \gamma, \quad \frac{\sqrt{Q}}{V} \approx \tan \gamma.$$

In this version the ratio is independent of  $B$  under the conditions of weak fields as well as strong ones. The equality of the amplitude ratio and  $\tan^2 \gamma$  is only approximate — the angle being determined is affected by velocities and other parameters. We tested the accuracy of this approximation by calculating  $\gamma$  from the ratios  $\sqrt{Q}/V$  for four lines and comparing the calculated values with the model ones.

Figures 4a, b show the variations of  $\gamma$  along the simulation region, and Figs 4c, d show  $\gamma$  as a function of  $B$ . The inclination is  $5\text{--}10^\circ$  within a range of 300 km in the central part of the first flux tube and  $10\text{--}20^\circ$  in the second flux tube. This is in accord with the data of [19], where an analysis of the V, Q profiles in plages gave an inclination of flux tubes no less than  $10^\circ$ . As judged from the distribution  $\gamma(B)$  found with the use of the Stokes diagnostics (Fig. 4d), there are no fields weaker than 20 mT, but such fields cannot be detected by the method based on the measurements of the V-profile peaks. It is also obvious from Fig. 4d that there are no longitudinal fields with  $B < 160$  mT and  $\gamma < 10^\circ$ . This is likely to be a result of the limitedness of the method used to determine  $\gamma$ . Besides, the angles  $\gamma$  found with the use of the Fe I 1564.8 nm line are greater than the angles determined from the lines in the visible range. Hence we may conclude that the ratio  $\sqrt{Q}/V$  for the visible lines gives angles overestimated by  $10^\circ$ , and the overestimation is even greater for the IR line. The method we used here is simple and quite reliable, as the distribution  $\gamma(B)$  obtained by it is in agreement with the model distribution. In reality, when  $\chi \neq 0$ , we have to use the relation  $(Q^2 + U^2)^{1/2}/V^2 \approx \tan^2 \gamma$ .

## 4.3 Radial velocities in magnetic elements

As of now, there are no observations which would prove the existence of stationary vertical flows with velocities higher than 250 m/s (average from numerous observations) inside

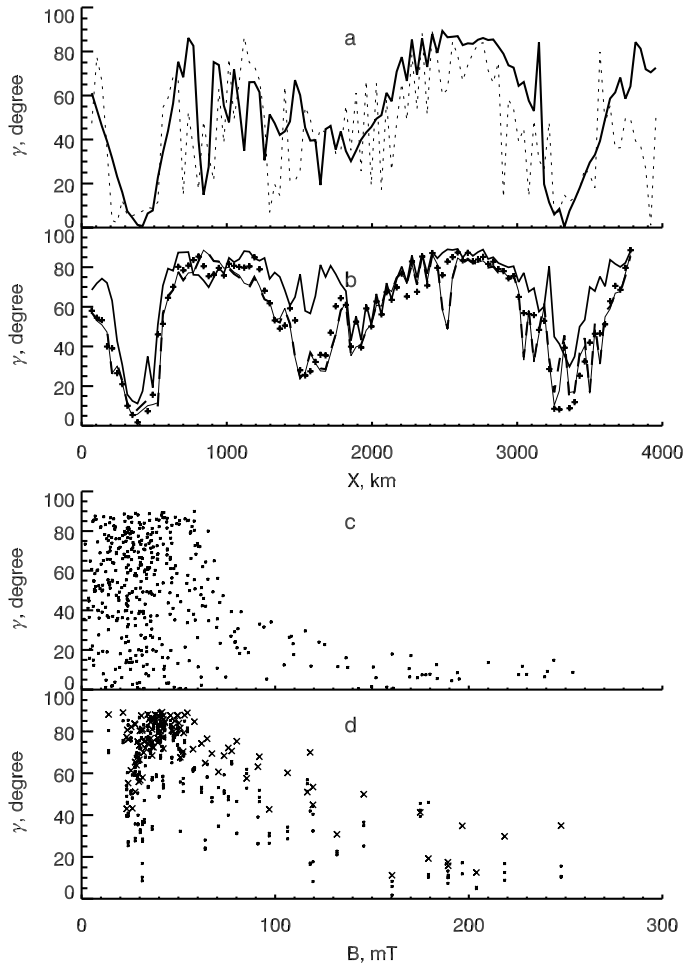


Fig. 4(a, b). Magnetic field inclination along the simulation region: a) from a MHD snapshot at the levels  $\log \tau_R = 0$  (solid line) and  $\log \tau_R = -2$  (dotted line), b) from the amplitude ratio  $\sqrt{Q}/V$  for four lines. Note the data derived from  $\lambda 524.7$  nm (thin line) and  $\lambda 525.02$  nm (dashed line) are almost the same. The remaining symbols are the same as in Fig. 3c, d.

Fig. 4(c, d). The inclination  $\gamma$  vs. magnetic field intensity: c) from a MHD snapshot at four  $\log \tau_R$  levels — 0, -1, -2, and -3; d)  $\gamma$  from the amplitude ratio  $\sqrt{Q}/V$  for four lines (crosses correspond to  $\lambda 1564.8$  nm). Here  $B$  was derived from the distance between the V peaks of the  $\lambda 1564.8$  nm line.

small-scale magnetic elements [18]. Considerable line shifts are sometimes observed in individual magnetic elements. The nature of the V-profile shifts still remains unknown and is always a topical problem in the studies of the structure and dynamics of flux tubes. The horizontal distribution of vertical velocities displayed in Fig. 5a was obtained directly from the MHD models. A velocity minimum (about 0 km/s) is observed at the center of the first flux tube, while maxima of 6 and 9 km/s can be seen at a distance of 100 km from the tube center; then the velocity falls sharply again. Such the distribution suggests the existence of very sharp horizontal gradients which may be a consequence of a relatively big step (35 km) in our numerical simulation. In actuality the velocities are smoother, but just the same, they strongly differ from the velocities in the nonmagnetic neighborhood. In observations the velocity may be underestimated because it heavily depends on spatial averaging due to low spatial resolution and atmospheric and instrumental distortions.

The velocities  $v_I$ ,  $v_Q$ ,  $v_V$ , which were found from the I, V, and Q profiles calculated for four lines, were compared with the model velocities (Fig. 5). The best agreement was found for the velocities measured as shifts of the  $\pi$ -components of Q profiles (Fig 5d), except the cases when  $\gamma = 0$ ,  $Q = 0$  (flux tube center), and shifts of the zero crossing of V profiles, except the cases of multicomponent V profiles (Fig 5c). The velocities obtained from the shifts of the I-profile center for the IR line ((Fig 5b)) deviate strongly from the true (model) velocities at sites with strong magnetic fields. As the I profile splits completely into  $\sigma$ -components of various amplitudes, the risk of mistaking the wavelength of a strong  $\sigma$ -component for the wavelength of the line core is run when the central wavelength of the line is determined automatically from the central intensity minimum.



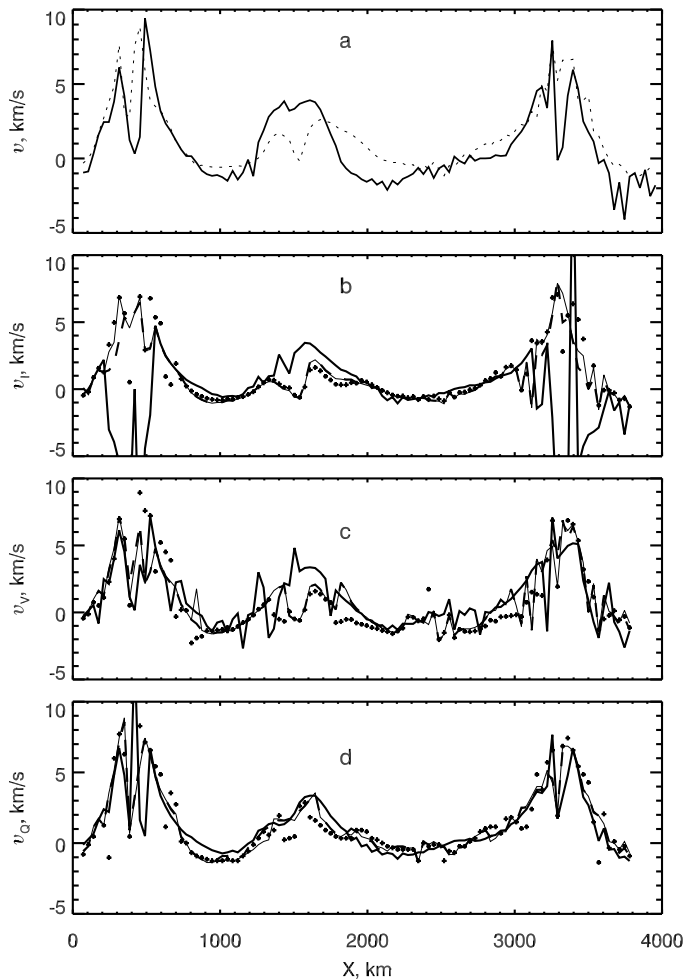


Fig. 5. Vertical velocity along the simulation region: a) from the MHD model at the levels  $\log \tau_R = 0$  (solid line) and  $\log \tau_R = -2$  (dotted line); b, c, d) shifts of the I, V, and Q profiles of four lines, respectively. Designations are the same as in Fig. 3c, d.

So, the vertical velocities inside flux tubes are determined quite reliably from the shifts of Q and V profiles. The velocity should not be determined in the automatic mode from the shifts of the I profiles of IR lines with large Landé factors.

#### 4.4 Temperature

The temperature diagnostics in small-scale magnetic features is carried out with the use of the temperature line ratio (TLR). This quantity was used for the first time when the true weakening of the I profile of the line Fe I 525.02 nm with respect to the line Fe I 523.30 nm inside unresolved magnetic elements was studied [10]. Ideally, the lines in the TLR must have different temperate sensitivities and close central depths  $d_c$ , wavelengths, and effective Landé factors  $g_{\text{eff}}$ . With the ratio between the amplitudes  $a_V$  of their V profiles, we can estimate the line weakening associated with temperature variations in a region with magnetic fields, i.e., in a flux tube. At elevated temperatures the sensitive line is weakened to a greater degree and TLR is less than unity, and vice versa. To obtain temperature from this ratio, it should be calibrated by model calculations, as it is done for the magnetic line ratio MLR.

For lines in the visible spectrum, the ratio

$$\text{TLR} = \frac{a_V(524.71)g_{\text{eff}}(525.06)}{a_V(525.06)g_{\text{eff}}(524.71)} = \frac{1.5}{2} \cdot \frac{a_V(524.71)}{a_V(525.06)}$$

is often used in actual practice. It does not meet all the requirements, as the line pa-

rameters are not always close to one another, and so we introduced a coefficient which equalizes the amplitudes of V profiles. This coefficient is approximately equal to 1.11 on the assumption that  $a_V \approx d_c$ . We calculated TLR (with a coefficient of 1.11) for our MHD model (Fig. 6). It depends not only on temperature, but on the vertical temperature gradients and the magnetic and temperature saturation in the lines as well, and this distorts the results of the diagnostics. In the central regions of flux tubes the magnetic saturation of the lines Fe I 524.7 and 525.06 nm is very strong. The amplitude  $a_V$  is temperature-insensitive there, and the method fails (TLR  $\approx 1$ ); TLR  $> 1$  at flux tube periphery, where the saturation drastically decreases. Hence it follows that the TLR method for temperature diagnostics inside flux tubes is not sufficiently reliable because of line saturation effects, especially in those cases when the spatial resolution is high. The central depths of these two lines become highly saturated in the regions with lower temperatures and become less sensitive to temperature variations.

The continuum brightness is also often used as a temperature indicator. Figure 6b shows the profiles of normalized continuum intensity along the horizontal coordinate, or the contrast  $I_c/\langle I_c \rangle$ . The intensity  $I_c$  was calculated for each model column in the continuum of two lines Fe I 525.0 and 1564.8 nm,  $\langle I_c \rangle$  being the intensity averaged in the horizontal direction over the whole simulation region. Observations suggest that the contrast in small magnetic elements heavily depends on spatial resolution. Magnetic elements less than 300 km in size have a small brightness (1.1–1.4 in the network), and the elements larger than 300 km have a darker continuum (0.7–0.9 in plages). For IR lines, no brightening is observed even in small magnetic elements, while darkening is typical of larger elements. This occurs because the IR lines near  $\lambda = 1650.0$  nm have a minimum in the continuum opacity.

The contrasts calculated for the MHD models at Fe I 525.0 and 1564.8 nm (dotted line and solid line, respectively, in Fig. 6b) are very different, the horizontal gradients being much higher in the visible spectrum. The contrast changes sharply at the center of the stronger flux tube — from 0.5 to 1.3, on the average, in the visible spectrum and from 0.8 to 1.0 in the infrared. The temperature at the level  $\log \tau_R = 0$  changed from 5700 to 6400 K at the center of the same flux tube (Fig. 6a). Our calculations are in accord with the brightness variations observed in the continuum in magnetic features.

## 5 Spatial averaging effect in the Stokes diagnostics

It is well known that not only the amplitudes and asymmetries of the measured Stokes Q, U, and V profiles but the areas of the profile wings and shifts as well depend on the spatial, temporal, and spectral resolution. The reason is the spatial and temporal averaging as well as the instrumental and atmospheric distortions of the signal measured. Simulations of the spatial smearing made with the use of the modulation transfer function (which allows for the atmospheric and telescopic distortions) reveal that the contrast in the continuum of a flux tube 100 km in diameter may be by a factor of 7–8 higher than the contrast measured with a 0.3'' resolution. At present the spatial resolution is not better than 0.25–0.3'' (180–220km), and the reliability of the parameters measured in thin flux tubes still remains a problem. Calculating the V profiles for various intervals along the simulation region in the MHD models, we may study the spatial averaging effect on these profiles. The averaged profiles may have several components with widely different parameters depending on horizontal temperature gradients, vertical velocities, magnetic field intensities, inclinations, and polarities. The well-known shape of V profiles may be

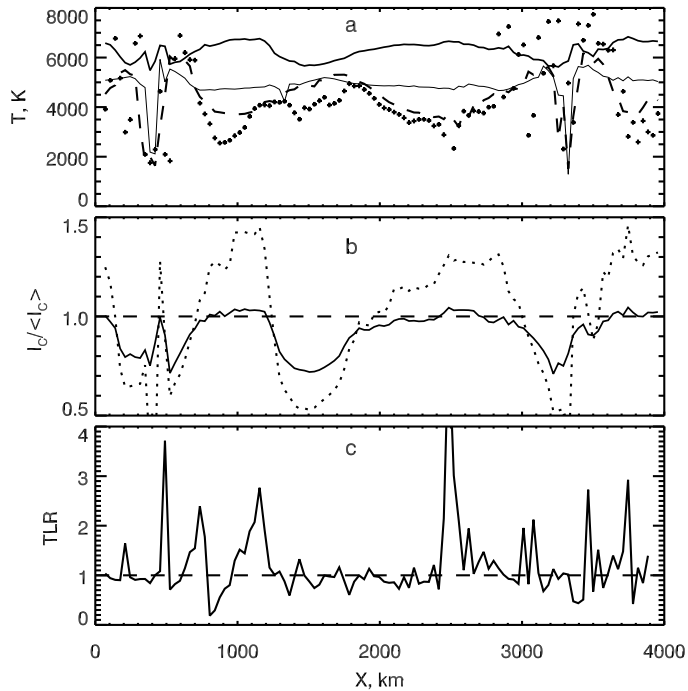


Fig. 6. Temperature distribution along the simulation region: a) from the MHD model at the levels  $\log \tau_R = 0$  (thick line),  $\log \tau_R = -1$  (thin line),  $\log \tau_R = -2$  (dashed line), and  $\log \tau_R = -3$  (plusses); b) continuum contrast at  $\lambda 525.0$  nm (dotted line) and  $\lambda 1564.8$  nm (thick line); c) method of temperature line ratio.

distorted in this case, and the application of the Stokes diagnostics becomes questionable.

The problem is illustrated in Fig. 7, where we plotted the amplitudes  $a_V$  and the parameters  $B_{rb}$ ,  $v_V$ ,  $v_Q$  derived from the V and Q profiles of the line Fe I 1564.8 nm in spectral scans with varying spatial resolution: about 35, 70, 200, 600, 1000, 1300, and 4000 km. The spatial variations in the velocity and the magnetic field intensity and polarity demonstrated in Fig. 2 can be compared with the diagnostics results plotted in Fig. 7. The V profiles will be affected by spatial resolution until very high resolutions are attained. At a 35-km resolution the derived values of  $B_{rb}$ ,  $v_V$ ,  $v_Q$  coincide quite well with the model values. When the V profile consists of two or more components, the distortions of the profile at low resolutions markedly affect the determination of the amplitude  $a_V = (a_b + a_r)/2$  (Fig. 7a), the distances between the peaks (Fig. 7b), and the zero-crossing shifts (Fig. 7c). The spatial averaging drastically degrades the accuracy of the Stokes diagnostics at resolutions lower than 200 km ( $\approx 0.3''$ ), especially in the regions with steep horizontal gradients. As an example, we give the velocities derived from the shifts of the profiles calculated for the spectral scans with different resolutions from 0 to 1300 km in the simulation region. We obtained 0.4, -1, 2.4, 0.5, -0.5, and 0 km/s for six scans with a 200-km resolution, 0.6, -0.2 km/s for two scans with a 600-km resolution, and 0 km/s for one scan with a 1300-km resolution. The highest velocity obtained with a resolution of  $0.3''$  (200 km) was four times greater than the velocity obtained with a resolution of  $1''$  (600 km). Hence it follows that the choice of spatial resolution strongly affects the results of Stokes diagnostics with the use of V profiles.

## 6 Conclusion

We demonstrated with the use of the Stokes diagnostics that new 2-D MHD models [6] are in accord with observations and may be successfully used to study magnetoconvection in the solar photosphere. We also tested the methods of Stokes diagnostics of small-scale magnetic elements. The results are as follows.

The IR line  $\lambda 1564.8$  nm of Fe I is more suitable for the testing than the Fe I lines

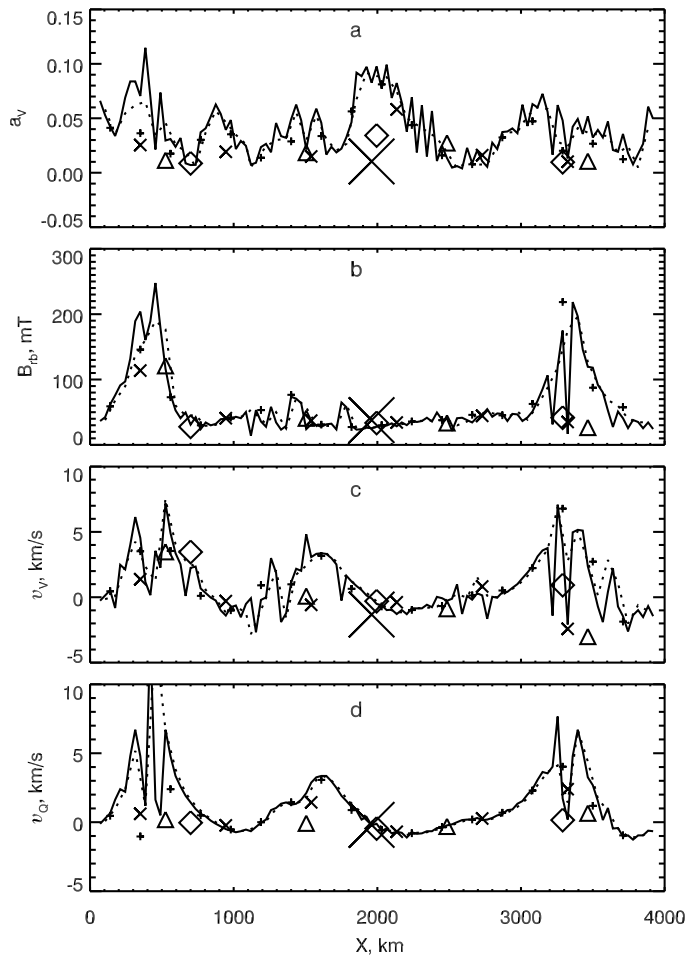


Fig. 7. Effect of spatial averaging on the results of Stokes diagnostics, a) amplitude  $a_V$ ; b) field intensity  $B_{rb}$ ; c, d) shifts of V and Q profiles. Horizontal averaging of profiles: 35 km (solid line), 70 km (dotted line), 200 km (plusses), 600 km (crosses), 1000 km (triangles), 1300 km (diamonds); the entire region (big cross).

$\lambda$  524.71 and 525.02 nm. Being less temperature-sensitive, it is less prone to saturation, and its high magnetic sensitivity does not decrease inside flux tubes at low temperatures.

The magnetic field intensity is estimated most reliably from the measurements of the distances between the V-profile peaks in the IR lines with large Landé factors. The lower sensitivity limit of this method is about 20 mT. When we want to determine the longitudinal field intensity only, the method of the center of masses may be used with confidence for any magnetic lines. Large longitudinal magnetic fields (0.1 T) are detected with confidence from the magnetic line ratio ( $MLR < 0.7$  at the flux tube center).

The inclination of magnetic field vector can be determined directly from the amplitude ratio  $\tan^2 \gamma \approx (Q^2 + U^2)^{1/2} / V^2$  with an accuracy of  $10^\circ$ . Longitudinal fields ( $\gamma < 10^\circ$ ,  $B < 160$  mT) cannot be measured by this method.

The velocities of vertical motions inside magnetic elements are reliably determined from the shifts of the  $\pi$ -components in the Q profiles and the zero crossings of V profiles. When the V profiles are of anomalous shape because of the presence of regions with opposite polarities, the shift of the  $\pi$ -components of Q profiles should be used.

The temperature in flux tubes with high spatial resolution cannot be reliably estimated from the temperature line ratio for two lines in the visible spectrum due to strong magnetic and temperature saturation of lines in flux tubes.

Spatial averaging significantly affects the Stokes diagnostics of flux tubes. Resolutions worse than 200 km may produce erroneous results. The reason has to do with the horizontal gradients of parameters inside flux tubes.

**Acknowledgements.** We are indebted to A. S. Gadun for furnishing the MHD models

for the Stokes profile calculations and S. K. Solanki for furnishing the observations as well as for useful discussion of the results and their comments. The study was partially financed by the Swiss National Science Foundation (Grant No. 7UKPJ 48440).

## References

- [1] I. N. Atroshchenko and V. A. Sheminova, “Numerical simulation of the interaction between solar granules and small-scale magnetic fields,” *Kinematika i Fizika Nebes. Tel [Kinematics and Physics of Celestial Bodies]*, vol. 12, no. 4, pp. 32–45, 1996.
- [2] L. R. Bellot Rubio, B. Ruiz Cobo, and M. Collados, “Flux-tube model atmospheres and Stokes V zero-crossing wavelengths,” *Astrophys. J. Lett.*, vol. 478, no. 1, pp. L45–L48, 1997.
- [3] P. N. Bernasconi, C. U. Keller, H. P. Povel, and J. O. Stenflo, “Direct measurements of flux tube inclinations in solar plages,” *Astron. and Astrophys.*, vol. 302, no. 2, pp. 533–542, 1995.
- [4] P. N. Brandt, A. S. Gadun, and V. A. Sheminova, “Absolute shifts of Fe I and Fe II lines in solar active regions (disk center),” *ibid.*, vol. 13, no. 5, pp. 75–86, 1997.
- [5] S. B. F. Dorch and Å. Nordlund, “Numerical 3D simulations of buoyant magnetic flux tubes,” *ibid.*, vol. 338, no. 1, pp. 329–339, 1998.
- [6] A. S. Gadun, V. A. Sheminova, and S. K. Solanki, “Formation of small-scale magnetic elements: surface mechanism,” *ibid.*, vol. 15, no. 5, pp. 387–397, 1999.
- [7] U. Grossmann-Doerth, M. Schüssler, and S. K. Solanki, “Stokes V asymmetry and shift of spectral lines,” *ibid.*, vol. 221, no. 2, pp. 338–341, 1989.
- [8] U. Grossmann-Doerth, M. Schüssler, and O. Steiner, “Convective intensification of solar surface magnetic fields: Results of numerical experiments,” *ibid.*, vol. 337, no. 3, pp. 928–939, 1998.
- [9] J. W. Harvey and D. Hall, “Magnetic field observations with Fe I  $\lambda$  1564.8 nm,” *Bull. Amer. Astron. Soc.*, vol. 7, no. 3, p. 459, 1975.
- [10] J. W. Harvey and W. Livingston, “Magnetograph measurements with temperature-sensitive lines,” *Solar Phys.*, vol. 10, no. 2, pp. 283–293, 1969.
- [11] E. Landi Degl’Innocenti, “MALIP – a programme to calculate the Stokes parameter profiles of magnetoactive Fraunhofer lines,” *Astron. and Astrophys. Suppl. Ser.*, vol. 25, no. 1, pp. 379–390, 1976.
- [12] K. Muglach and S. K. Solanki, “Infrared lines as probes of solar magnetic features. I. A many-line analysis of a network region,” *Astron. and Astrophys.*, vol. 263, no. 1/2, pp. 301–311, 1992.
- [13] A. K. Pierce and J. B. Breckinridge, *The Kitt Peak Table of Photographic Solar Spectrum Wavelengths*, Kitt Peak Nat. Obs. Contr., no. 559, 1973.

- [14] J. Sanchez Almeida, “Physical properties of the solar magnetic photosphere under the MISMA hypothesis: I. Description of the inversion procedure,” *Astrophys. J.*, vol. 491, no. 2, pp. 992–1008, 1997.
- [15] M. D. Semel, “Contribution a l’etude des champs magnetiques dans les regions actives solaires,” *Ann. d’Astrophys.*, vol. 30, pp. 513–522, 1967.
- [16] V. A. Sheminova, *Calculating Profiles of the Stokes Parameters of Magnetically Sensitive Absorption Lines in Stellar Atmospheres* [in Russian], Kiev, 1990 (VINITI File No. 2940–V90, 30 May 1990).
- [17] S. K. Solanki, “Small-scale solar magnetic fields: an overview,” *Space Sci. Rev.*, vol. 31, pp. 1–188, 1993.
- [18] S. K. Solanki, “Dynamics of flux tubes in the solar atmosphere: observations,” in: *Solar and Heliospheric Plasma Physics (Lecture Notes in Physics)*, C. E. Alissandrakis, G. Simnett, and L. Vlahos (Editors), pp. 49–73, Springer, Berlin, 1997.
- [19] S. K. Solanki, C. Keller, and J. O. Stenflo, “Properties of solar magnetic flux tubes from only two spectral lines,” *Astron. and Astrophys.*, vol. 188, no. 1, pp. 183–197, 1987.
- [20] S. K. Solanki, I. Rüedi, and W. Livingston, “Infrared lines as probes of solar magnetic features. II. Diagnostic capabilities of Fe I 1564.8.5 Å and 15652.9 Å,” *ibid.*, vol. 263, no. 1/2, pp. 312–322, 1992.
- [21] S. K. Solanki, O. Steiner, M. Bünte, et al., “On the reliability of Stokes diagnostics of magnetic elements away from solar disc centre,” *ibid.*, vol. 333, no. 2, pp. 721–731, 1998.
- [22] J. O. Stenflo, “Magnetic-field structure of the photospheric network,” *Solar Phys.*, vol. 32, no. 1, pp. 41–63, 1973.
- [23] J. O. Stenflo and J. W. Harvey, “X-ray resonance scattering in a spherically symmetric coronal model,” *ibid.*, vol. 95, no. 1/2, pp. 99–109, 1985.
- [24] J. O. Stenflo, J. W. Harvey, J. W. Brault, and S. K. Solanki, “Diagnostics of solar magnetic fluxtubes using a Fourier transform spectrometer,” *Astron. and Astrophys.*, vol. 131, no. 2, pp. 333–346, 1984.